Journal of Earth Science, *Vol. 31*, *No. 6*, *p. 1183–1189*, *December 2020* *ISSN 1674-487X*
Printed in China
https://doi.org/10.1007/s12583-020-1338-2

An Investigation of Dislocation in Olivine Phenocrysts from the Hawaiian Basalts

Zhuo-Yue Li[1], **Da-Peng Wen**[1], **Yong-Feng Wang***[1, 2], **Xiangwen Liu***[3]
1. *School of Earth Sciences*, *State Key Laboratory of Geological Processes and Mineral Resources*, *China University of Geosciences*, *Wuhan* 430074, *China*
2. *Global Tectonic Center*, *School of Earth Sciences*, *China University of Geosciences*, *Wuhan* 430074, *China*
3. *Engineering Research Center of Nano-Geo Materials of Ministry of Education*, *China University of Geosciences*, *Wuhan* 430074, *China*
Zhuo-Yue Li: https://orcid.org/0000-0002-6475-4878; Yong-Feng Wang: https://orcid.org/0000-0003-2236-7893;
Xiangwen Liu: https://orcid.org/0000-0002-5761-7509

ABSTRACT: Intracrystalline distortions (like undulose extinction, dislocations, and subgrain boundaries) in olivine from naturally-deformed peridotites are generally taken as signs of dislocation creep. However, similar features in olivine phenocrysts that have been found in basaltic magmas are still not well understood. In particular, whether subgrain boundaries in olivine phenocrysts arise from plastic deformation or grain growth is still debated (in the latter case, they are essentially grain boundaries but not subgrain boundaries. Therefore, we used hereinafter subgrain-boundary-like structures instead of subgrain boundaries to name this kind of intracrystalline distortion). Here we carried out a detailed study on dislocations and subgrain-boundary-like (SG-like) structures in olivine phenocrysts from two Hawaiian basaltic lavas by means of petrographic microscopy, scanning electron microscopy, and transmission electron microscopy (TEM). Abundant and complex dislocation substructures (free dislocations, dislocation walls, and dislocation tangles) were observed in the decorated olivine grains, similar to those in olivine from peridotite xenoliths entrained by the Hawaiian basalts. The measured average dislocation density is $(2.9\pm1.3)\times10^{11}$ m^{-2}, and is three to five orders of magnitude higher than that in laboratory-synthesized, undeformed olivine. TEM observations on samples cut across the SG-like structures by FIB (focused ion beam) demonstrated that this kind of structures is made of an array of dislocations. These observations clearly indicate that these structures are real subgrain boundaries rather than grain boundaries. These facts suggest that the observed high dislocation densities and subgrain boundaries cannot result from crystal crystallization/growth, but can be formed by plastic deformation. These deformation features do not prove that the olivine phenocrysts (and implicitly mantle xenoliths) were deformed after their capture by the basaltic magmas, but can be ascribed to a former deformation event in a dunitic cumulate, which was formed by magmatic fractionation, then plastically deformed, and finally disaggregated and captured by the basaltic magma that brought them to the surface.
KEY WORDS: olivine phenocryst, dislocation, subgrain boundary, deformation, Hawaiian basalts.

0 INTRODUCTION

Olivine is volumetrically dominant (commonly >60 %) and probably the weakest mineral in the Earth's upper mantle. It is therefore believed to control the rheological behavior of the upper mantle (Mackwell et al., 1990). During mantle convection, olivine can shape significant intragranular plastic deformation features, such as various dislocation substructures, undulose extinction, and subgrain boundaries. These features can in turn be used to acquire knowledge about how mantle flow proceeds, and also provide part of the necessary link between experimental and natural deformation processes. For instance, dislocation characteristics of olivine within orogenic, xenolithic and ophiolitic peridotites have been extensively studied to gain insight into the deformation mechanism (Park and Jung, 2014; Wang et al., 2013; Green and Radcliffe, 1972) and magnitude of differential stress (Cao et al., 2017; Toriumi, 1979; Durham et al., 1977) prevailing in the upper mantle.

Significant intracrystalline plastic deformation, in addition to strong crystallographic preferred orientation (CPO), in olivine from naturally-deformed mantle peridotites has been generally considered as a robust indicator of dislocation-creep deformation by many previous studies (e.g., Tommasi and Ishikawa, 2014; Soustelle et al., 2010). Intracrystalline distortions, such as dislocation substructures and SG-like structures, are often observed in olivine phenocrysts that crystallized from basalts as well (e.g., Welsch et al., 2013; Sakyi et al., 2012; Vinet and Higgins, 2010). However, disagreements remain whether these features reflect

*Corresponding author: yfwang@cug.edu.cn; xwliu@cug.edu.cn

Manuscript received November 3, 2019.
Manuscript accepted May 11, 2020.

plastic deformation or not. For example, Sakyi et al. (2012) suggested based upon dislocation observations of olivine phenocrysts from the Hawaiian basalts that these olivine phenocrysts were plastically deformed prior to their entrainment in the host magma. In contrast, Welsch et al. (2013) argued that olivine phenocrysts containing the SG-like structures are derived from dendritic growth and ripening rather than plastic deformation.

If, as suggested by Welsch et al. (2013), the SG-like structures in olivine phenocrysts are due to dendritic growth, one would expect that there are no dislocations in these boundaries and few within the grain interiors. On the other hand, if these SG-like structures arise from plastic deformation, then dislocations should be abundant in these boundaries and grain interiors. Therefore, whether the olivine phenocrysts from basaltic magmas contain abundant dislocations (especially in their SG-like structures) is key to resolve the above-mentioned disputes. However, few efforts have been made to reveal the dislocation features and no attempts have been made to illustrate the dislocation features in the SG-like structures in basalt-borne olivine phenocrysts so far.

The purpose of this study is to clarify whether olivine phenocrysts that crystallized from basaltic magmas contain abundant dislocations, and especially, whether the SG-like structures in these olivine phenocrysts are of deformation origin. To this end, we carried out a detailed investigation of dislocation substructures in olivine phenocrysts from two Hawaiian basalts by means of optical microscopy and SEM (scanning electron microscopy) observations of decorated olivine. In particular, we also used transmission electron microscopy (TEM) to analyze the dislocation features in grain interiors and SG-like structures of olivine prepared by the traditional ion thinning method and the novel focused ion beam (FIB) method, respectively.

1 SAMPLES AND METHODS

The two Hawaiian basalt samples, one from the O'ahu Island and the other from the Big Island, used for this study had been previously investigated by Wen et al. (2018). They are both tholeiitic lavas with SiO_2 of 46.99 wt.%–47.38 wt.% and Na_2O+K_2O of 1.49 wt.%–2.61 wt.% (Wen et al., 2018). The major-element compositions of the olivine phenocrysts from these two basalts were also reported by Wen et al. (2018).

To reveal dislocation substructures in the olivine phenocrysts, we first employed the oxidation decoration technique following Kohlstedt et al. (1976). The basic principle of this method is that during firing in air, FeO in olivine is oxidized to Fe_2O_3, which precipitates at dislocations and thus making them visible using optical microscopy or SEM. This method had been widely used to investigate dislocation substructures in naturally and experimentally deformed olivine (Park and Jung, 2014; Hanson and Spetzler, 1994; Bai and Kohlstedt, 1992; Gueguen, 1977). The detailed procedure for dislocation decoration in this study is as follows. The samples were first cut to rock slabs of ~3.5×2×1 cm^3 and polished on one side (~3.5×2 cm^2 in area) to within 0.05 μm using alumina slurry. The rock slabs were then put into a muffle furnace with the polished surface upward. The temperature was increased to 900 ºC with a ramp rate of ~7 ºC/min and hold for 30 min. After slowly cooled down to room temperature, the rock slabs were taken out and attached with their polished surface to glass slides using epoxy resin. The thin sections were then prepared in sequence by cutting, grinding, and polishing to within 0.05 μm using alumina slurry.

Our observations of dislocations were made by a combination of optical and SEM, with the latter greatly improving the spatial resolution (Karato and Sato, 1982). SEM observations of dislocations were conducted using a Quanta 450 field emission gun scanning electron microscope housed at the State Key Laboratory of Geological Processes and Mineral Resources, China University of Geosciences (Wuhan) (GPMR-CUGW). The operating conditions are an acceleration voltage of 15 kV and a beam current of 20 nA. To reveal the intracrystalline misorientation, we also performed electron backscatter diffraction (EBSD) analyses on the decorated olivine grains. EBSD patterns were collected automatically by a NordlysNano detector and processed using the Aztec software. The operation conditions during EBSD analyses were a working distance of 23–25 mm, an accelerating voltage of 20 kV, and a spot size of 6.

The traditional TEM specimens were prepared by a Gatan 656 dimple grinder and a Gatan-600 ion mill for physical and ion thinning, respectively. In addition, we also used FIB technique to prepare TEM specimens to reveal dislocation features in the SG-like structures. The ultra-microstructures of olivine were observed using a Philips CM12 transmission electron microscopy (TEM) at an accelerating voltage of 120 kV, which yields a point-to-point resolution of 0.34 nm and a line resolution of 0.2 nm.

To estimate the free dislocations density in olivine phenocrysts, 31 electron backscattered images of different positions covering all the decorated thin sections were taken by SEM at a 6 000× magnification. These images were then processed using ImageJ (http://rsbweb.nih.gov/ij/) following the method detailed in Farla et al. (2010). SG-like structures/dislocation walls were excluded in measuring dislocation density. The 3D dislocation density (ρ) was calculated as

$$\rho = \left(\frac{1}{A}\right)\sum\left[\sqrt{1+\left(\frac{l_0}{d}\right)^2}\right] \quad (1)$$

where A is the total area imaged, l_0 is the true dislocation line length, and d=6.2×10^{-7} m was used at 15 kV in this study (Farla et al., 2010).

2 RESULTS

The phenocrysts in the studied samples are mainly composed of randomly-oriented olivine, clinopyroxene, and minor plagioclase (Fig. 1a). The olivine phenocrysts are euhedral and tabular with a grain size of 0.5–2.5 mm and an average axial ratio of 1.6±0.3. Some of them contain inclusions of basaltic glass or plagioclase. SG-like structures are often observed in these olivine phenocrysts (Figs. 1b–1d). No intracrystalline deformation is observed in the clinopyroxene grains.

Under a petrographic microscope, the decorated olivine shows abundant dislocations, which are reddish brown (Fig. 2). In addition, the decorated olivine phenocrysts also show variable and complex dislocation substructures, including free dislocations (i.e., randomly distributed, isolated dislocations that are not organized into a dislocation wall), dislocation walls (i.e., a

linear array of well-organized dislocations), dislocation tangles (i.e., a pile of dislocations that are intricately interwoven). The average (geometric mean) density of free dislocation was estimated to be $(2.9\pm1.3)\times10^{11}$ m^{-2} using high-resolution backscattered electron images (Fig. 3). There is no significant difference in the dislocation density between coarse and fine olivine phenocrysts, although dislocations are heterogeneously distributed within each olivine grain. EBSD mappings show that olivine develops SG-like structures with an internal misorientation of 3º–7º, which are nearly coincident with those revealed by the oxidation decoration technique (Fig. 4). We also used the method detailed in Soustelle and Manthilake (2017) to determine the slip systems of dislocations in these SG-like structures. Analyses of 14 olivine grains show that the active slip systems can be grouped into two categories with equal amounts, i.e., the (010)[100] and the (001)[100] slip systems.

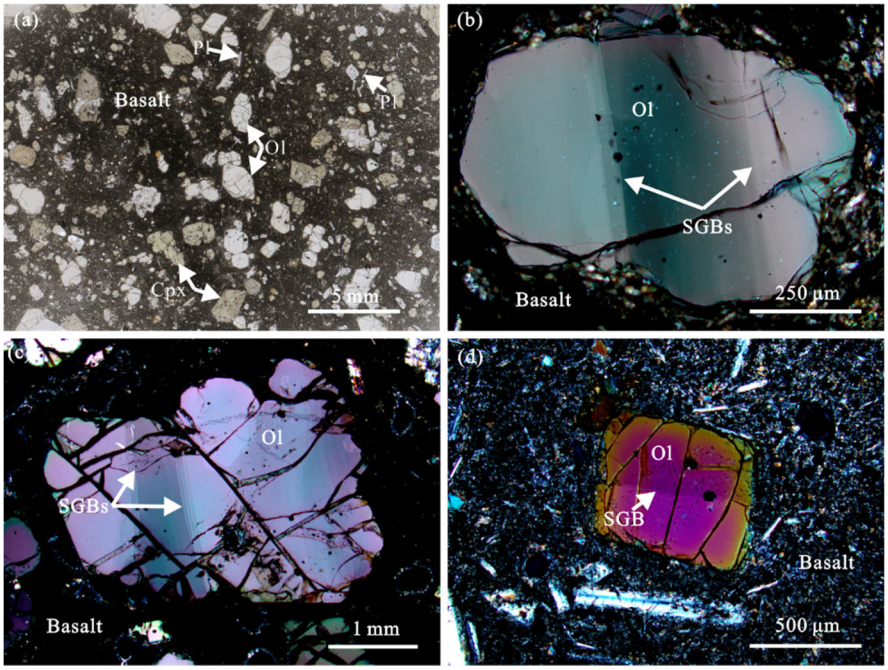

Figure 1. Microphotographs showing petrography and microstructures of olivine phenocrysts from the Hawaiian basalts. (a) Photomicrograph showing the petrographic features of the Hawaiian basalts (plane polarized light). Note the abundant euhedral olivine phenocrysts. (b)–(d) SG-like structures (SGBs) in the olivine phenocrysts (cross polarized light). Cpx. Clinopyroxene; Ol. olivine; Pl. plagioclase.

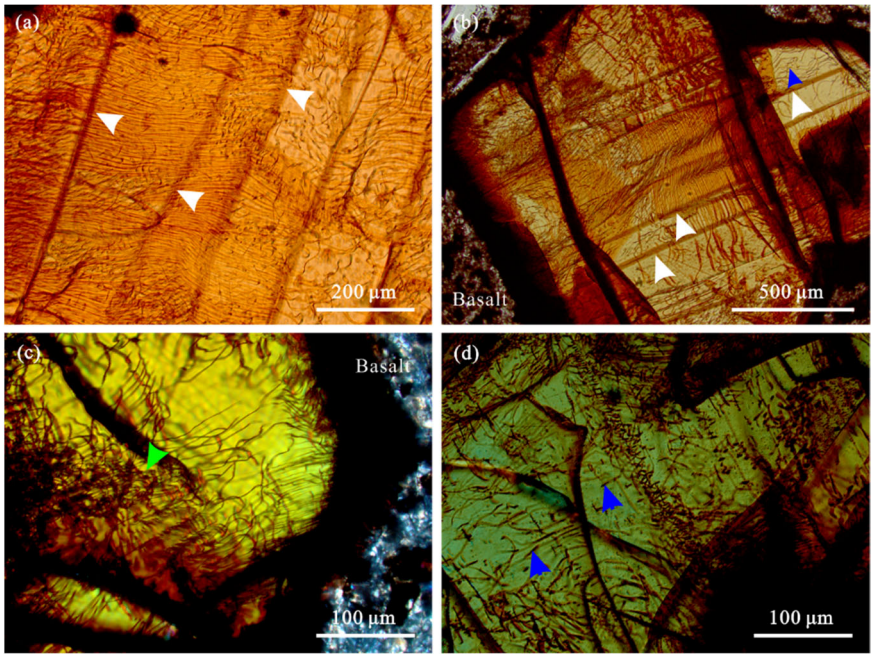

Figure 2. Photomicrographs showing dislocation substructures in the decorated olivine phenocrysts from the Hawaiian basalts. Plane polarized light. (a) Dislocation walls (white arrows); (b) dislocation walls (white arrows) and free dislocations (blue arrow); (c) dislocation tangle (green arrow); (d) free dislocations (blue arrows).

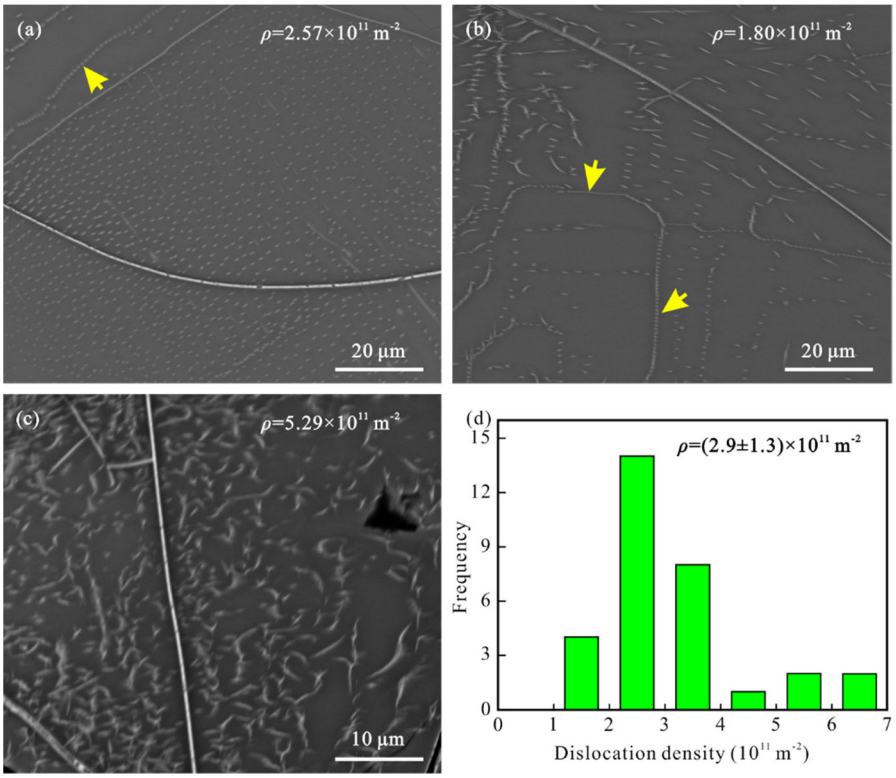

Figure 3. Estimation of dislocation densities in the decorated olivine phenocrysts. (a)–(c) Backscattered electron images showing various dislocation densities within different olivine grains, yellow arrows indicate the dislocation walls, which are excluded during measurements of dislocation density; (d) histogram showing the dislocation density distribution and the average (geometric mean) dislocation density for the studied samples.

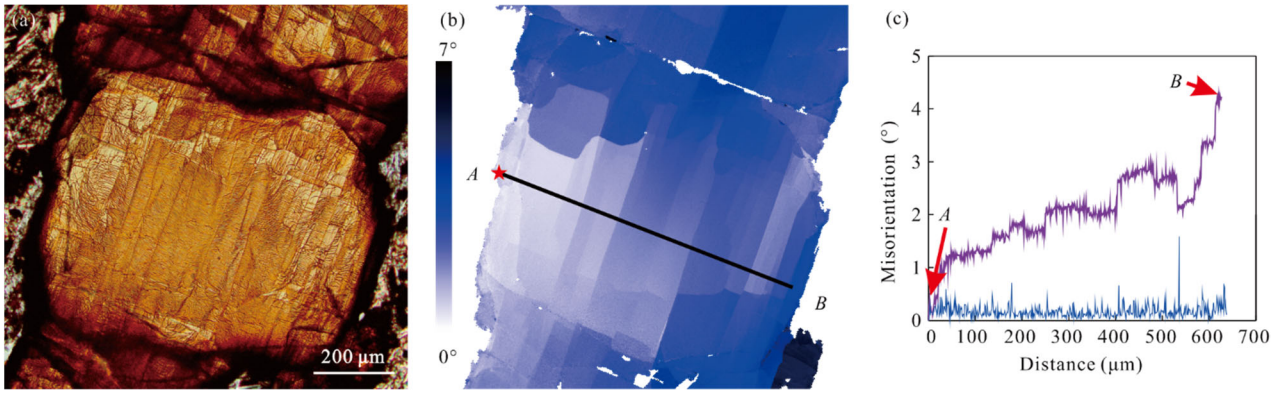

Figure 4. Typical EBSD results of the decorated olivine phenocrysts. (a) Photomicrograph showing the olivine phenocryst after decoration, plane polarized light; (b) orientation map showing the internal misorientation of the olivine phenocryst in (a) relative to the reference point (indicated as a red star), note that this image illustrates subgrain boundaries in the olivine phenocryst almost the same as those in the decorated one; (c) diagram showing the continuous change of misorientation angle from point to point (violet line) and with respect to the first point (blue line) along the profile *AB* in (b).

TEM observations (Fig. 5) showed dislocation substructures comparable to those revealed by the oxidation decoration method, including edge dislocations, dislocation walls and dislocation tangles. Analyses of slip systems for 4 free dislocations show that the slip systems are exclusively (010)[100]. In particular, our observations show that the SG-like structures in studied olivine are essentially composed of an array of well-organized dislocations (Fig. 5e).

3 DISCUSSION AND CONCLUSION

The low $Mg^{\#}$ [=the molar ratio of $100\times Mg/(Mg+Fe^{2+})$; <86], euhedral crystal form, and inclusions of basaltic glass or plagioclase in olivine phenocrysts all point to that these olivine grains were crystallized products from the magma rather than relics of captured mantle peridotites (Wen et al., 2018). However, these olivine phenocrysts contain a considerable amount of dislocations, with an average dislocation density of $(2.9\pm1.3)\times10^{11}$ m^{-2}. This value is comparable to those (10^{10}–10^{11} m^{-2}) determined for deformed olivine within peridotite xenoliths from Hawaii (Gueguen and Darot, 1980; Gueguen, 1977), but is three to five orders of magnitude higher than those synthetic, undeformed olivine from experiments (Hanson and Spetzler, 1994; Hanson et al., 1991; Hosoya and Takei, 1982). In addition, in contrast to undeformed olivine synthesized in laboratory

(Hanson and Spetzler, 1994), which is characterized mainly by a few straight dislocations and dislocation tangles, the decorated olivine phenocrysts show more variable and complex dislocation substructures. These dislocation features are indistinguishable from those observed by previous studies in olivine from mantle xenoliths (Gueguen, 1977), indicative of dislocation creep as the dominant deformation mechanism (Green and Radcliffe, 1972). EBSD mapping of decorated olivine also revealed evident internal misorientation consistent with deformation occurring by the motion of dislocations. These facts suggest that dislocations within the studied olivine phenocrysts could not be ascribed to the crystallization processes.

Sakyi et al. (2012) investigated the dislocation substructures of olivine phenocrysts in three Hawaiian basaltic lavas (Kilauea, Mauna Loa, and Koolau). They identified two types of olivine grains with distinct morphology: one is blocky (deformed) and the other is rod-shaped (undeformed). The blocky olivine shows regularly-shaped dislocation substructures and high dislocation densities ($>10^{10}$ m^{-2}), whereas the rod-shaped olivine shows extremely low dislocation densities ($<7\times10^{6}$ m^{-2}). Combined with other petrographic and compositional features, the authors concluded that the rod-shaped olivine crystals should have formed during rapid cooling of the host magmas, while the blocky olivine grains are relics of dunitic cumulates formed by an earlier magmatic fractionation. The plastic deformation of the blocky olivine phenocrysts was inherited from those of the dunitic cumulates in the presence of interstitial melt (Sakyi et al., 2012). Because the dislocation substructures and densities in the blocky olivine is quite similar to those of olivine phenocrysts in this study, we considered that the observed dislocation substructures probably have the same origin as those in Sakyi et al. (2012), i.e., they reflected a former deformation event in a dunitic cumulate. This inference is reasonable considering that olivine phenocrysts are more competent than basaltic magmas and should not be plastically deformed after their entrapment by the magmas. The rod-shaped olivine was not observed in our samples; they were only observed in the picritic lavas (Sakyi et al., 2012).

SG-like structures in olivine phenocrysts that crystallized from basaltic magmas are not uncommon (e.g., Welsch et al., 2013; Vinet et al., 2011; Helz, 1987). Although several previous studies have suggested that the olivine phenocrysts containing SG-like structures were plastically deformed crystals derived from tectonized dunites (e.g., Vinet et al., 2011; Clague and Denlinger, 1994; Herz, 1987), Welsch et al. (2013) argued that these structures resulted from lattice mismatches caused by dendritic growth, rather than by plastic deformation. In fact, the so-called "subgrain boundaries" in Welsch et al. (2013) are grain

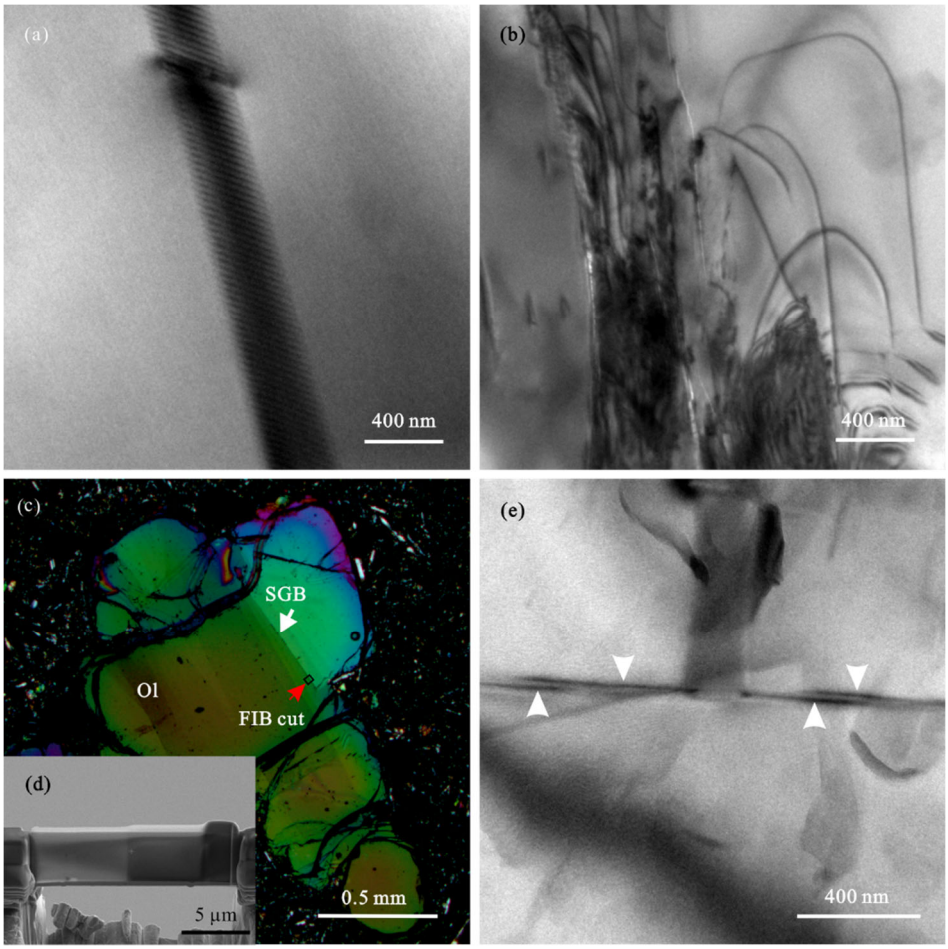

Figure 5. TEM-revealed dislocation features in the olivine phenocrysts. (a) Dislocation walls; (b) dislocation tangle; (c) photomicrograph showing the position (black rectangle) where a FIB cut was made to analyze the dislocation features in the SG-like structure (SGB); (d) micrograph showing the sample prepared by FIB; (e) the SG-like structure was made of organized dislocations (white arrows). Ol. Olivine.

boundaries between some misaligned, independent olivine crystals that form parallel grouping and happen to have up to 15º misalignments. Strictly speaking, they are only SG-like structures but not real subgrain boundaries. By implication, no dislocations are expected to present in these boundaries. In contrast, our TEM observations on samples cut by FIB across the SG-like structures clearly demonstrated that these structures are composed of regularly organized dislocations. This strongly indicates that these structures are caused by dislocation motion through dislocation climb (Davis et al., 2011) and are real subgrain boundaries. Most likely, the subgrain boundaries and dislocations in the studied olivine phenocrysts were generated by the same deformation event (s) that was (were) superimposed on the former dunitic cumulates. Therefore, these deformation features cannot be taken as evidence that mantle xenoliths entrained by basaltic magmas do not faithfully preserve mantle deformation. In a word, the dislocations and subgrain boundaries in olivine phenocrysts from our studied samples both originated from plastic deformation rather than crystal crystallization/growth.

The slip systems inferred based on analyses of subgrain boundaries and of free dislocations using TEM are different: the former reveals both (010)[100] and (001)[100] and the latter reveals only (010)[100] as the dominant slip system(s). This discrepancy suggests that the dislocations in the subgrain boundaries may not be representative of the most active slip systems during deformation. A similar conclusion has also been drawn based on detailed microstructural studies of olivine from peridotite xenoliths by several previous studies (e.g., Zaffarana et al., 2014; Soustelle et al., 2010; Falus et al., 2008). If we accept that the slip system determined by TEM represents the true active slip system during deformation of the olivine phenocrysts, then it can be concluded that these olivine grains were probably deformed under high temperature, low stress, and relatively dry conditions (e.g., Jung and Karato, 2001).

Based on the above discussion, we revised the model for the formation of the olivine phenocrysts from the Hawaiian basalts proposed by Wen et al. (2018). In Wen et al. (2018), the olivine phenocrysts were interpreted as direct crystallization products from the host basaltic magma. In contrast, we considered here that the olivine phenocrysts, at least the studied ones, most likely originated from a former dunitic cumulate that formed by a former magmatic fractionation. This cumulate was subsequently plastically deformed, leading to intracrystalline deformation features within the olivine grains, followed by disaggregation and capture by the hosting magma. Euhedral and low-$Mg^{\#}$ olivine from cumulates have been frequently reported in literature (e.g., Tribuzio et al., 2008; Müntener and Piccardo, 2003; Nielsen, 1981). Therefore, the low-$Mg^{\#}$ and euhedral characters of the olivine phenocrysts most likely were inherited from their precusor olivine grains in the dunitic cumulate. However, this new model does not affect the major conclusions in Wen et al. (2018).

ACKNOWLEDGMENTS

We thank Prof. Junfeng Zhang for providing us the samples and Haijun Xu for maintaining the SEM and EBSD systems. Professor Tao Chen is greatly thanked for her help during sample preparation by FIB. Insightful comments by two anonymous reviewers are helpful to improve the manuscript and acknowledged. This work was sponsored by the National Natural Science Foundation of China (Nos. 41590623, 41972231, 41872230). The final publication is available at Springer via https://doi.org/10.1007/s12583-020-1338-2.

REFERENCES CITED

Bai, Q., Kohlstedt, D. L., 1992. High-Temperature Creep of Olivine Single Crystals, 2. Dislocation Structures. *Tectonophysics*, 206(1/2): 1–29. https://doi.org/10.1016/0040-1951(92)90365-d

Cao, Y., Jung, H. Y., Song, S. G., et al., 2017. Olivine Fabrics and Tectonic Evolution of Fore-Arc Mantles: A Natural Perspective from the Songshugou Dunite and Harzburgite in the Qinling Orogenic Belt, Central China. *Geochemistry*, *Geophysics*, *Geosystems*, 18(3): 907–934. https://doi.org/10.1002/2016gc006614

Clague, D. A., Denlinger, R. P., 1994. Role of Olivine Cumulates in Destabilizing the Flanks of Hawaiian Volcanoes. *Bulletin of Volcanology*, 56(6/7): 425–434. https://doi.org/10.1007/s004450050052

Davis, G. H., Reynolds, S. J., Kluth, C. F., 2011. Structural Geology of Rocks and Regions. Wiley, New York. 176–178

Durham, W. B., Goetze, C., Blake, B., 1977. Plastic Flow of Oriented Single Crystals of Olivine: 2. Observations and Interpretations of the Dislocation Structures. *Journal of Geophysical Research*, 82(36): 5755–5770. https://doi.org/10.1029/jb082i036p05755

Falus, G., Tommasi, A., Ingrin, J., et al., 2008. Deformation and Seismic Anisotropy of the Lithospheric Mantle in the Southeastern Carpathians Inferred from the Study of Mantle Xenoliths. *Earth and Planetary Science Letters*, 272(1/2): 50–64. https://doi.org/10.1016/j.epsl.2008.04.035

Farla, R. J. M., Kokkonen, H., Fitz Gerald, J. D., et al., 2010. Dislocation Recovery in Fine-Grained Polycrystalline Olivine. *Physics and Chemistry of Minerals*, 38(5): 363–377. https://doi.org/10.1007/s00269-010-0410-3

Green, H. W. II, Radcliffe, S. V., 1972. Dislocation Mechanisms in Olivine and Flow in the Upper Mantle. *Earth and Planetary Science Letters*, 15(3): 239–247. https://doi.org/10.1016/0012-821x(72)90169-0

Gueguen, Y., 1977. Dislocations in Mantle Peeidotite Nodules. *Tectonophysics*, 39(1/2/3): 231–254. https://doi.org/10.1016/0040-1951(77)90098-1

Gueguen, Y., Darot, M., 1980. Microstructures and Stresses in Naturally Deformed Peridotites, In: Scheidegger, A. E., ed., Tectonic Stresses in the Alpine-Mediterranean Region. Springer, Vienna. 159–172

Hanson, D. R., Spetzler, H. A., 1994. Transient Creep in Natural and Synthetic, Iron-Bearing Olivine Single Crystals: Mechanical Results and Dislocation Microstructures. *Tectonophysics*, 235(4): 293–315. https://doi.org/10.1016/0040-1951(94)90191-0

Hanson, D. R., Young, M., Ryerson, F. J., 1991. Growth and Characterization of Synthetic Iron-Bearing Olivine. *Physics and Chemistry of Minerals*, 18(1): 53–63. https://doi.org/10.1007/bf00199044

Helz, R., 1987. Diverse Olivine Types in Lava of the 1959 Eruption of Kilauea Volcano and Their Bearing on Eruption Dynamics. *U.S. Geological Survey Professional Paper*, 1350: 691–722

Hosoya, S., Takei, H., 1982. Floating-Zone Growth of Single-Crystal Olivine [$(Mg_{1-X}Fex)_2SiO_4$]. *Journal of Crystal Growth*, 57(2): 343–348. https://doi.org/10.1016/0022-0248(82)90489-4

Jung, H., Karato, S. I., 2001. Water-Induced Fabric Transitions in Olivine. *Science*, 293(5534): 1460–1463. https://doi.org/10.1126/science.1062235

Karato, S. I., Sato, H., 1982. Effect of Oxygen Partial Pressure on the

Dislocation Recovery in Olivine: A New Constraint on Creep Mechanisms. *Physics of the Earth and Planetary Interiors*, 28(4): 312–319. https://doi.org/10.1016/0031-9201(82)90088-7

Kohlstedt, D. L., Goetze, C., Durham, W. B., et al., 1976. New Technique for Decorating Dislocations in Olivine. *Science*, 191(4231): 1045–1046. https://doi.org/10.1126/science.191.4231.1045

Mackwell, S. J., Bai, Q., Kohlstedt, D. L., 1990. Rheology of Olivine and the Strength of the Lithosphere. *Geophysical Research Letters*, 17(1): 9–12. https://doi.org/10.1029/gl017i001p00009

Müntener, O., Piccardo, G. B., 2003. Melt Migration in Ophiolitic Peridotites: The Message from Alpine-Apennine Peridotites and Implications for Embryonic Ocean Basins. *Geological Society*, *London*, *Special Publications*, 218(1): 69–89. https://doi.org/10.1144/gsl.sp.2003.218.01.05

Nielsen, T. F. D., 1981. The Ultramafic Cumulate Series, Gardiner Complex, East Greenland. *Contributions to Mineralogy and Petrology*, 76(1): 60–72. https://doi.org/10.1007/bf00373684

Park, Y., Jung, H., 2014. Deformation Microstructures of Olivine and Pyroxene in Mantle Xenoliths in Shanwang, Eastern China, near the Convergent Plate Margin, and Implications for Seismic Anisotropy. *International Geology Review*, 57(5/6/7/8): 629–649. https://doi.org/10.1080/00206814.2014.928240

Sakyi, P. A., Tanaka, R., Kobayashi, K., et al., 2012. Inherited Pb Isotopic Records in Olivine Antecryst-Hosted Melt Inclusions from Hawaiian Lavas. *Geochimica et Cosmochimica Acta*, 95: 169–195. https://doi.org/10.1016/j.gca.2012.07.025

Soustelle, V., Manthilake, G., 2017. Deformation of Olivine-Orthopyroxene Aggregates at High Pressure and Temperature: Implications for the Seismic Properties of the Asthenosphere. *Tectonophysics*, 694: 385–399. https://doi.org/10.1016/j.tecto.2016.11.020

Soustelle, V., Tommasi, A., Demouchy, S., et al., 2010. Deformation and Fluid-Rock Interaction in the Supra-Subduction Mantle: Microstructures and Water Contents in Peridotite Xenoliths from the Avacha Volcano, Kamchatka. *Journal of Petrology*, 51(1/2): 363–394. https://doi.org/10.1093/petrology/egp085

Tommasi, A., Ishikawa, A., 2014. Microstructures, Composition, and Seismic Properties of the Ontong Java Plateau Mantle Root. *Geochemistry*, *Geophysics*, *Geosystems*, 15(11): 4547–4569. https://doi.org/10.1002/2014gc005452

Toriumi, M., 1979. Relation between Dislocation Density and Subgrain Size of Naturally Deformed Olivine in Peridotites. *Contributions to Mineralogy and Petrology*, 68(2): 181–186. https://doi.org/10.1007/bf00371899

Tribuzio, R., Tiepolo, M., Fiameni, S., 2008. A Mafic-Ultramafic Cumulate Sequence Derived from Boninite-Type Melts (Niagara Icefalls, Northern Victoria Land, Antarctica). *Contributions to Mineralogy and Petrology*, 155(5): 619–633. https://doi.org/10.1007/s00410-007-0261-1

Vinet, N., Flemming, R. L., Higgins, M. D., 2011. Crystal Structure, Mosaicity, and Strain Analysis of Hawaiian Olivines Using *in situ* X-Ray Diffraction. *American Mineralogist*, 96(4): 486–497. https://doi.org/10.2138/am.2011.3593

Vinet, N., Higgins, M. D., 2010. Magma Solidification Processes beneath Kilauea Volcano, Hawaii: A Quantitative Textural and Geochemical Study of the 1969–1974 Mauna Ulu Lavas. *Journal of Petrology*, 51(6): 1297–1332. https://doi.org/10.1093/petrology/egq020

Wang, Y. -F., Zhang, J. F., Shi, F., 2013. The Origin and Geophysical Implications of a Weak C-Type Olivine Fabric in the Xugou Ultrahigh Pressure Garnet Peridotite. *Earth and Planetary Science Letters*, 376: 63–73. https://doi.org/10.1016/j.epsl.2013.06.017

Welsch, B., Faure, F., Famin, V., et al., 2013. Dendritic Crystallization: A Single Process for All the Textures of Olivine in Basalts?. *Journal of Petrology*, 54(3): 539–574. https://doi.org/10.1093/petrology/egs077

Wen, D. -P., Wang, Y. -F., Zhang, J. F., et al., 2018. Anisotropic Growth of Olivine during Crystallization in Basalts from Hawaii: Implications for Olivine Fabric Development. *American Mineralogist*, 103(5): 735–741. https://doi.org/10.2138/am-2018-6174

Zaffarana, C., Tommasi, A., Vauchez, A., et al., 2014. Microstructures and Seismic Properties of South Patagonian Mantle Xenoliths (Gobernador Gregores and Pali Aike). *Tectonophysics*, 621: 175–197. https://doi.org/10.1016/j.tecto.2014.02.017